Journal of Medicinal and Chemical Sciences 7 (2024) 538-554

Journal of Medicinal and Chemical Sciences

Journal homepage: http://www.jmchemsci.com/

Original Article

Investigation of Calcium Carbonate Porogen on Methylene Blue Adsorption in Alginate Cellulose Xanthate Beads from Corn Stalks

Eny Yulianti[1], Nanang Qazim[1], Anton Prasetyo[1], Siska Ela Kartika[1], Muhajidin Ahmad[2], Rahadian Zainul[3]*, Azril[4], Herland Satriawan[5], Ahmad Zikri[6], Mohammad Abdullah[7]

[1]*Department of Chemistry, Faculty of Science and Technology, Universitas Islam Negeri Maulana Malik Ibrahim, Malang, Indonesia, 65144*
[2]*Department of Chemistry, Faculty of Mathematics and Science, Universitas Negeri Padang, Padang, Indonesia*
[3]*Department of Biology, Faculty of Science and Technology, Universitas Islam Negeri Maulana Malik Ibrahim, Malang, Indonesia, 65144*
[4]*Department of Biomedical Engineering, National Cheng Kung University, Tainan City, Taiwan*
[5]*Institute of Ocean and Earth Sciences, University of Malaya, 50603, Kuala Lumpur, Malaysia*
[6]*Department of Mechanical Engineering, Faculty of Engineering, Bursa Uludag University, Bursa 16850, Türkiye*
[7]*Chemical Engineering Studies, College of Engineering, Universiti Teknologi MARA Johor Branch, Pasir Gudang Campus, Bandar Seri Alam, 81750 Masai, Pasir Gudang, Johor Bahru, Johor, Malaysia*

ARTICLEINFO

Article history
Receive: 2023-09-28
Received in revised: 2023-11-17
Accepted: 2023-11-29
Manuscript ID: JMCS-2310-2352
Checked for Plagiarism: **Yes**
Language Editor:
Dr. Fatima Ramezani
Editor who approved publication:
Dr. Rassoul Dinarvand

DOI:10.26655/JMCHEMSCI.2024.3.9

KEYWORDS
Corn stalk
Methylene blue
Cellulose xanthate
Ionic gelation
Porogen

ABSTRACT

Corn stalk can be used as a potential adsorbent because of its abundance, cost-effectiveness, and accessible functional groups that allow chemical modifications. This study aims to synthesize cellulose xanthate alginate beads (ACX beads) from corn stalks to remove methylene blue from aqueous solutions. ACX beads with various doses of porogen $CaCO_3$ were printed using the ionic gelation method, and then characterized using FTIR, optical microscopy, and SEM-EDX. The results of the FTIR analysis reported changes in the C-S, C=S, and S-C-S vibrations that indicated the xanthate formation. Furthermore, as the porogen dose increased, the OH intensity decreased. The high intensity of the OH group results in a high swelling process. The results of the optical microscopy analysis showed that the porogen made the ACX beads spherical. SEM-EDX analysis showed that the higher the porogen dose, the rougher the surface morphology of the ACX beads and the larger the pore diameter. The maximum adsorption capacity was obtained on ACX beads without porogen with a contact time of 360 hours. The study reveals that the kinetic adsorption followed a pseudo-second-order kinetic model proposed chemical adsorption. The larger the porogen, the more crosslinks between the divalent cations and alginate or cellulose that are formed, inhibiting the bond between the ACX beads and water and methylene blue, thereby reducing the swelling process and the adsorption capacity of the ACX beads. In addition, the pore size that is too large does not match the size of the methylene blue molecule.

* Corresponding author: Rahadian Zainul
✉ E-mail: rahadianzmsiphd@fmipa.unp.ac.id

GRAPHICAL ABSTRACT

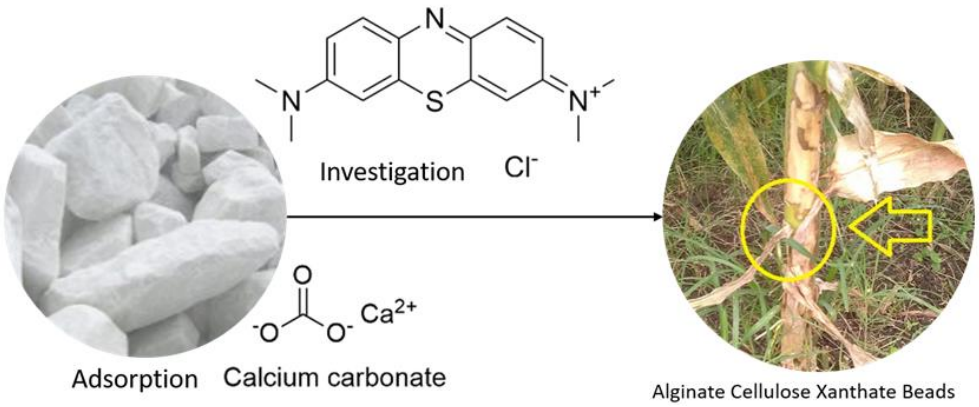

Introduction

Rapid industrial development has a positive effect in the form of an increase in the economic sector, as well as a negative impact on the condition of dangerous industrial waste, such as waste containing synthetic dyes. The food, paper, leather, textile, pharmaceutical, and paint industries commonly use this dye as a colorant. Approximately 7 × 105 tons of 1000 dyes and pigments are produced annually [1, 2].

These carcinogenic azo dyes cause unfavorable structural changes in the ecosystem when released into the aquatic environment. The eutrophication caused by this dye reduces the oxygen supply capacity of marine organisms and is extremely harmful to aquatic animals and plants. Toxic synthetic dyes in water pose ecological risks to the aquatic biota and can gradually accumulate in the human body through the food chain [3, 4]. Methylene blue can cause serious illnesses such as central nervous system toxicity, gastrointestinal infections, and discoloration of the brain parenchyma. As a result, removing dyes and other pollutants from the water reservoirs has become quite challenging and has been raising health and aquatic sustainability concerns among the scientific community for some time now [5, 6]. So far, many strategies have been proposed, including adsorption, coagulation, membrane filtration, ion exchange removal, photocatalytic degradation, biological/aerobic treatment, ozone treatment, and catalytic reduction to address this particular problem [7, 8]. The adsorption method is superior to the other dye wastewater treatment techniques because of its advantages, such as high efficiency, low cost, ease of operation, and less influence on harmful substances than other treatment method [9, 10]. The United States Environmental Protection Agency (USEPA) ranks adsorption as one of the best control methods [11].

Wastewater treatment uses various low-cost alternative adsorbents, such as agricultural solid waste, industrial solid waste, agricultural by-products, and biomass. For example, clay, mud, montmorillonite, hemp fibers, zeolites, and biochars (rice husks, pine wood, wheat, bagasse, switchgrass, and ficus calica bust) are used as adsorbents for the treatment of dye effluents in water areas [12, 13]. As the most abundant natural polymer, cellulose accounts for 40-50% of the earth's total biomass reserves. Up to 10 tonnes of cellulose produced by photosynthesis annually are considered as an inexhaustible green resource [14, 15].

Most cell walls of plants are composed of cellulose, hemicellulose, and lignin.

Cellulose is a strong molecule with a hydroxyl group, a monomer, in which repeating units of cellobiose units (disaccharide D-glucose) are bonded in 1, 4-bonds and open between adjacent glucose units of the same chain or different chains.

A linear polysaccharide with intermolecular hydrogen bonds exists in glucose. This compact hydrogen-bonded structure is a dense network of cellulose fibers that provides plant cell walls with antibacterial properties, toughness, and strength and is impervious to water and solvents [16, 17]. Hemicellulose is a monomer of pentose and hexose and is found in plant cell walls at about 20-35% of the dry weight of biomass. Lignin is present at a dry weight of approximately 10-25% and acts as a binder between the cellulose and hemicellulose components [18, 19]. The chemical functionalization of cellulose is carried out via the skeleton's hydroxyl group (OH). Various functional groups are bonded to cellulose mainly by esterification. The pathway chosen for this study was the deprotonation of hydroxyl groups under strongly alkaline conditions, followed by the formation of cellulose xanthate by a nucleophilic attack on carbon disulfide [20]. Like any xanthate, cellulose xanthate is insoluble in water, has a higher ion exchange or adsorption capacity than cellulose, and can be used to remove methylene blue [21]. The use of functionalized or modified cellulose to remove various contaminants from water, such as dyes, bacteria, toxic metal ions, or nanoparticulate drugs, has been extensively studied in the last few decades. Porous alginate-cellulose xanthate beads (ACX beads) made of cellulose, one of the most prevalent and affordable natural polymers, have been produced effectively [22, 23]. ACX beads are used to encapsulate active compounds. Of the several methods of encapsulating active compounds, ionic gelation is an interesting technique as it can be considered as a simple and easy method, is inexpensive, and does not require special equipment, high temperatures, and organic solvents [24]. Although many investigations have been performed to prepare adsorbents from corn stalks, significantly less research has been reported on the utilization of ACX beads from corn stalks for adsorption purposes. The current study aims to determine whether removing methylene blue from an aqueous solution is feasible using ACX beads. The effect of various operating parameters, including porogen dosage, contact time, and typical swelling behavior has been tested.

Materials and Methods

Corn stalks come from Sengkaling Malang Regency, sodium hydroxide (NaOH) p.a, hydrochloric acid (HCl) 37% p.a, carbon disulfide (CS_2) p.a, calcium carbonate ($CaCO_3$) p.a, sodium chlorite (NaClO2) p.a, acetic acid (CH_3COOH) p.a, zinc acetate ($Zn(CH_3CO_2)_2$), sodium alginate ($C_6H_7NaO_6$) p.a, methylene blue, and distilled water.

Extraction of cellulose from corn stalks

Corn stalks are cleaned and dried in the sun. The dried corn stalks were crushed and sieved at a size of 100 mesh. Furthermore, the corn stalks were dried at 60 °C for 24 h. A total of 50 g of corn stalks were immersed in 10% NaOH at 80 °C for 90 minutes. The pulp was washed with distilled water. The pulp was added with 1% $NaClO_2$ and 10% CH_3COOH at pH 5 at 75 °C for 60 minutes. Moreover, the pulp was washed with distilled water until a neutral pH was reached and hydrolyzed with 5% HCl at 90 °C for 60 minutes to obtain dispersed microfibers. Samples before and after cellulose extraction were characterized using FTIR.

Preparation of cellulose xanthate

Cellulose (5 g) was immersed in 20% NaOH for 3 h and allowed to stand at room temperature for 60 h. The cellulose was reacting with CS2. Furthermore, the cellulose was dissolved in 6% NaOH and shaken at a speed of 150 rpm at 25 ^oC for 3 h to obtain cellulose xanthate. Cellulose xanthate was characterized using FTIR (Varian Scimitar 1000) [25, 26].

Effect of porogen dosage

Sodium alginate (2 g) was dissolved in distilled water (40 mL) and reacted with 10% CH_3COOH until dissolved. The mixture was reacted with cellulose xanthate with a ratio of alginate: cellulose = 1:3. Then, the mixture was reacted with $CaCO_2$ (0.5, 1, 1.5 g) and dripped using a syringe into the crosslink (5% ($Zn(CH_3CO_2)_2$) and allowed to stand for 24 h. The ACX beads that formed were filtered and washed using distilled water. The ACX beads were reacted with HCl 1 mmol/L in a ratio of 1:8. The ACX beads were

shaken at 150 rpm for 45 minutes until no bubbles appeared. The resulting ACX beads were washed with distilled water until neutral pH was reached and dried at 37 °C for 24 h [27, 28].

Swelling of ACX beads

ACX beads (30 mg) immersed in distilled water (12 mL). The ACX beads were weighed at 3, 9, 12, and 24 h, and a swelling study was performed to determine the swelling behavior of the ACX beads. The analysis of the swelling behavior of the ACX beads was carried out with variations in the porogen dosage [29, 30].

Adsorption

The batch adsorption experiment measured the adsorption capacity of methylene blue on ACX beads. The adsorption capacity was determined by reacting 100 ppm methylene blue (10 mL) with ACX beads (1 mg) at various contact times of 24, 48, 93, 360, 384, and 408 h. A UV-Vis spectrophotometer (Varian Cary 50) was used to determine the methylene blue concentration at 665 nm [31, 32].

Results and Discussion

Preparation of ACX beads

This study synthesized ACX beads. The cellulose is derived from corn stalks and then modified into cellulose xanthate. ACX beads were printed using the ionic gelation method. Dried corn stalks were delignification using NaOH. Delignification causes a break in the bond between lignin and cellulose. NaOH can remove some components of lignin and hemicellulose [33, 34]. NaOH solution destroys and makes the previously strong and tightly bound fiber bonds disappear by breaking the cellulose structure. The breaking of hydrogen bonds between lignin with cellulose and hemicellulose was characterized by a significant decrease in lignin during treatment, resulting in the degradation of the fiber structure [35]. With NaOH, lignin is delignified, producing a black liquor-like filtrate that is dark brown and contains dissolved lignin, as displayed in Figure 1. It is still possible for cellulose from delignification to contain lignin, which has a brownish color, so bleaching is necessary. The bleaching agent used is $NaClO_2$ because it is stable at room temperature. The oxidizing agent ClO_2 can degrade lignin without damaging the cellulose structure. Cellulose, as a result of bleaching, is white, as shown in Figure 1. $NaClO_2$ solution can destroy lignin into simpler compounds and produce a permanent white color [36]. The weight of corn stalks powder produced after extraction decreased from 50 g to 31.37 g. The weight loss was due to the loss of non-cellulose compounds in corn stalks, such as hemicellulose and lignin, which had been hydrolyzed into simpler glucose.

The yield of cellulose produced was 37.26%. Cellulose has a reactive group in the form of hydroxyl (OH), which is dispersed uniformly on the cellulose side to create hydrogen bonds between cellulose molecules. Cellulose must be transformed into cellulose xanthate to remove the hydrogen bonds preventing cellulose from dissolving directly in water and other organic solvents. NaOH and CS_2 reagents are used to create cellulose xanthate. After adding these compounds, the xanthate group on cellulose will take the place of the hydroxyl group. The cellulose xanthate produced is orange in color [37, 38]. The dropping technique made ACX beads. This technique is done by dripping alginate cellulose xanthate into a zinc acetate solution using a syringe. The alginate cellulose xanthate composite was reacted with $CaCO_2$ as a porogen with variations of 0.5, 1, and 1.5 g to obtain ACX beads with the best pores. The ACX beads that had been left for 24 h were then washed using 1 mmol/L HCl for 45 minutes to remove $CaCO_2$. Subsequently, it was heated at 37 °C to remove the moisture content [39, 40].

Effect of porogen dosage

The difference in porogen dosage affects the swelling behavior of the ACX beads. With larger the porogen, the swelling process of the ACX beads is decreased. The greater the porogen, the more crosslinks between divalent cations and alginate or cellulose are formed, thereby inhibiting the bond between ACX beads and water, decreasing the ACX beads swelling process.

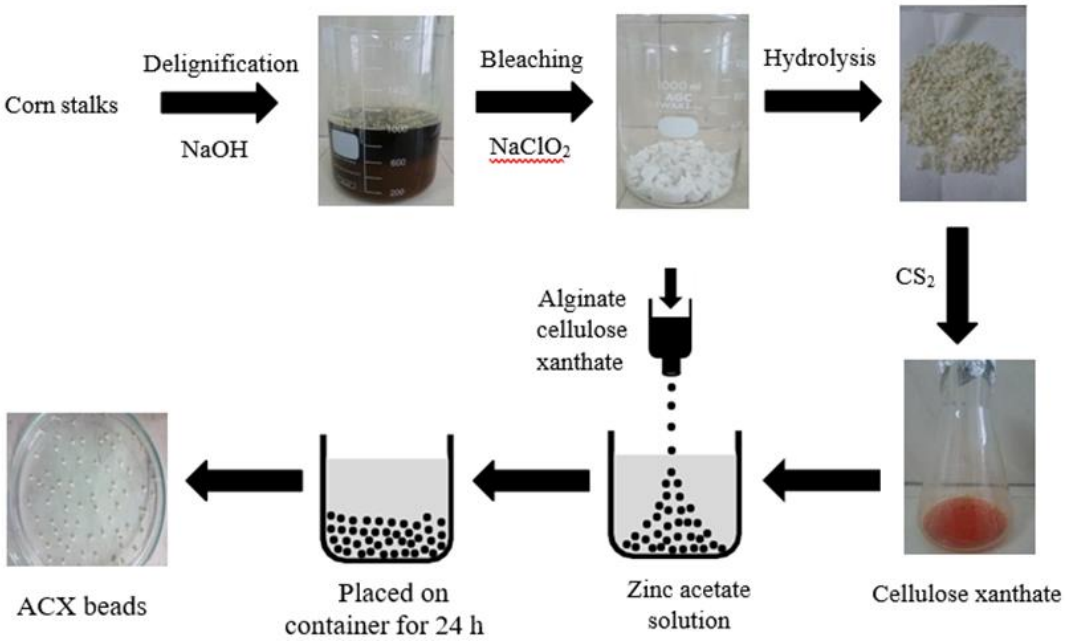

Figure 1: Preparation ACX beads

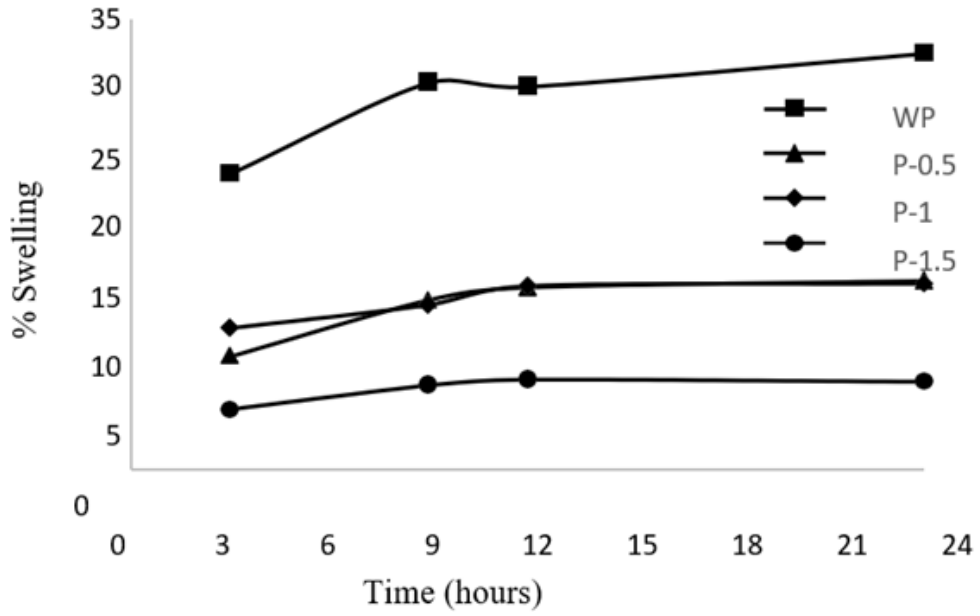

Figure 2: Swelling process ACX beads with the variation of porogen dosages and contact time

This is because alginate can crosslink with Ca^{2+} ions from the porogen. The diameter of ACX beads decreased with increasing porogen dosages of 5.57, 4.81, and 4.19 mm, respectively. These pores cause the ACX beads to swell longer so that less water is absorbed. In addition, the increase in porogen dosage makes the surface of the ACX beads rougher [41, 42].

Effect of contact time

The difference in contact time affects the swelling behavior of the ACX beads. The longer the contact time, the greater the ability of the ACX beads to absorb water. ACX beads with 1 and 1.5 g of porogen had an optimum time of 12 h. Conversion of polymer into gel matrix has reached the optimum point at 12 h. Diffusion occurs when the ACX beads have passed the optimum swelling point and the impermeable substance flows through the pores in the polymer matrix [43, 44].

Swelling of ACX beads

A swelling study was conducted to determine the adsorption ability of ACX beads. The swelling process of ACX beads was determined with variations in porogen dosage 0.5 g (P-0.5), 1 g (P-1), 1.5 g (P-1.5), and contact time 3, 9, 12, 24 h. Differences in porogen dosage and contact time affect the swelling process of the ACX beads. Based on Figure 2, the highest swelling process was found in ACX beads without porogen (WP) with a contact time of 24 h [45, 46].

Characterization

The characterization of ACX beads was performed using FTIR, an optical microscope, and SEM EDX. FTIR (Varian Scimitar 1000) to determine the functional groups formed, an optical microscope to determine the shape and diameter of ACX beads, and SEM-EDX (Hitachi TM 3000) to determine the surface morphology and elemental content [47, 48].

FTIR characterization

The functional groups of the ACX beads were examined utilizing FTIR in the wavenumbers range of 4000-400 cm^{-1}. Figure 3 illustrates the FTIR spectra of corn stalks powder, extracted cellulose, cellulose xanthate, and ACX beads. In the IR spectrum of the extracted cellulose, it can be seen that there was a change at 1457 cm^{-1} (C=C aromatic), 1251 cm^{-1} (CH2 symmetric bending), and 1049 cm^{-1} (C=O stretching). The loss of the wave number indicates the loss of lignin compounds. In the IR spectrum of cellulose xanthate, IR vibration peaks appeared at 520 cm^{-1} (C-S), 1000 cm^{-1} (C=S), and 1117 cm^{-1} (S-C-S), indicating the reaction of xanthate formation [49, 50]. According [51], wave numbers 580, 1030, and 1156 cm^{-1} indicate the presence of C-S, C=S, and S-C-S groups, which are xanthate groups. The wave number of corn stalk powder, extracted cellulose, and cellulose xanthate are summarized to provide a clear comparison of the changes in functional groups among these materials (Table 1). The spectra of IR ACX beads with variations in porogen dosages are depicted in Figure 4. The spectrum of IR ACX beads with porogen is different from that without porogen, namely at 3735 cm^{-1} (free OH) and 1303 cm^{-1} (C=C aromatic), which identified changes in the hydrophilic carrier functional groups [52].

Table 2 details the wave number of ACX beads with the variation of porogen dosage, highlighting these differences. According to [53], hydrophilicity is balanced by the presence of free carboxylic acid groups and hydroxyl groups inside the crosslink. According to [53], hydrophilicity is balanced by the presence of free carboxylic acid groups and hydroxyl groups inside the crosslink.

The wave number of 3447 cm^{-1} indicates the OH group in the ACX beads, and the intensity decreases with the addition of porogen. The OH group is a carrier of hydrophilic properties. Therefore, the higher intensity leads to higher hydrophilic properties. According to [54], the hydrophilic groups in the polymer network significantly affect swelling behavior and are crucial to swelling.

The OH group on the ACX beads had a high intensity, which resulted in a high swelling process. The group is derived from ACX beads, which can bind water molecules from the swelling process. The COOH group also has a hydrophilic nature at 1303 cm^{-1}. The wave number of 1303 cm^{-1} decreased with the addition of porogen to the ACX beads.

SEM-EDX characterization

The morphological changes on the surface of the ACX beads with the variation in porogen dosage were clarified by SEM-EDX. The SEM image is demonstrated in Figures 5 and 6. Accordingly, it can be seen that the ACX beads have a round shape and a rough surface. The round shape is produced by crosslinking alginate with divalent Zn^{2+} and Ca^{2+}. The formation of pores causes the rough surface of the ACX beads. From the SEM image, it can also be seen that the ACX beads have fold-shaped pores. Porogen is added to form pores in ACX beads. The range of these pore diameters is systematically documented in Table 3. Pore diameter range of ACX beads, providing a comprehensive view of how the pore sizes vary with different porogen dosages.

Table 1: The wave number of corn stalk powder, extracted cellulose, and cellulose xanthate

Vibration	Corn stalk powder	Extracted cellulose	Cellulose xanthate
OH *stretching*	3750 3445	- 3448	- 3451
CH aliphatic (sp^3)stretching	2928	2923	-
C=O *stretching*	1650	1649	1648
C=C aromatis	1508 1457	1540 -	- -
CH2 symmetricbending	1384 1251	1384 -	1385 -
S-C-S	-	-	1117
C=O *stretching*	1049	-	-
C=S	-	-	1000
Beta-glycoside bond	668	668	668
C-S	-	-	520

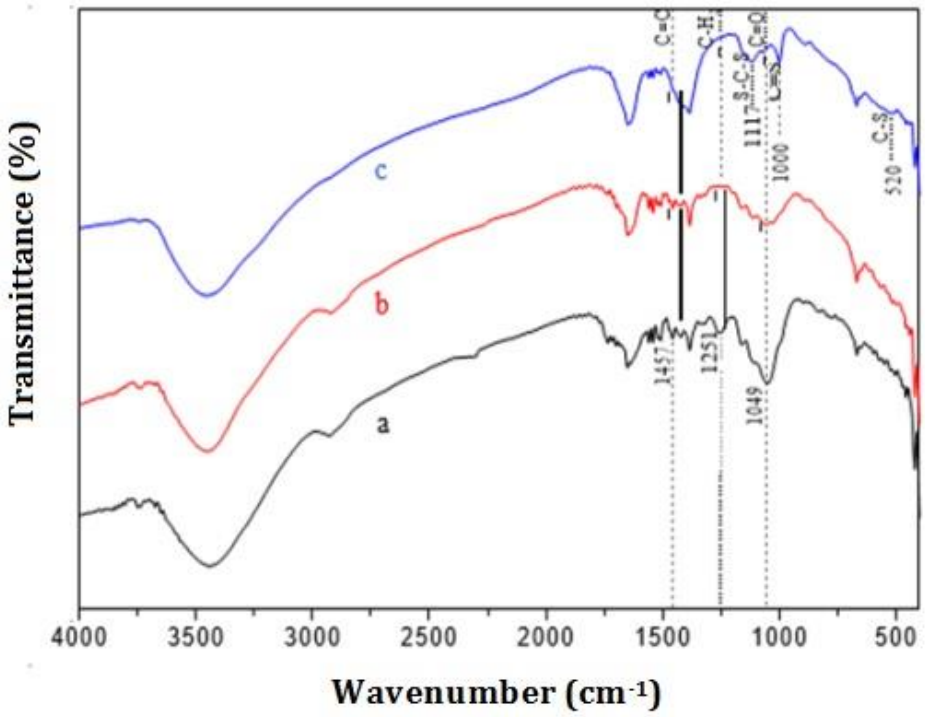

Figure 3: FTIR spectra (a) corn stalk powder, (b) extracted cellulose, and c. cellulose xanthate

Table 2: The wave number of ACX beads with the variation of porogen dosage

Vibration	Without porogen	Porogen 0.5 g	Porogen 1 g	Porogen 1.5 g
OH *stretching*	3854 3735 3447	3854 3736 3447	3854 3736 3447	3854 3736 3447
CH aliphatic (sp^3)stretching	2930	2929	-	-
C=O *stretching*	1635	1618	1620	1617
C=C aromatis	1417	1425	1425	1425
C-O-C *stretching*	1303	1303	1303	1303
C-H stretching out of plane of aromatic ring	-	876	876	876
OH *bending*	816	817	-	818

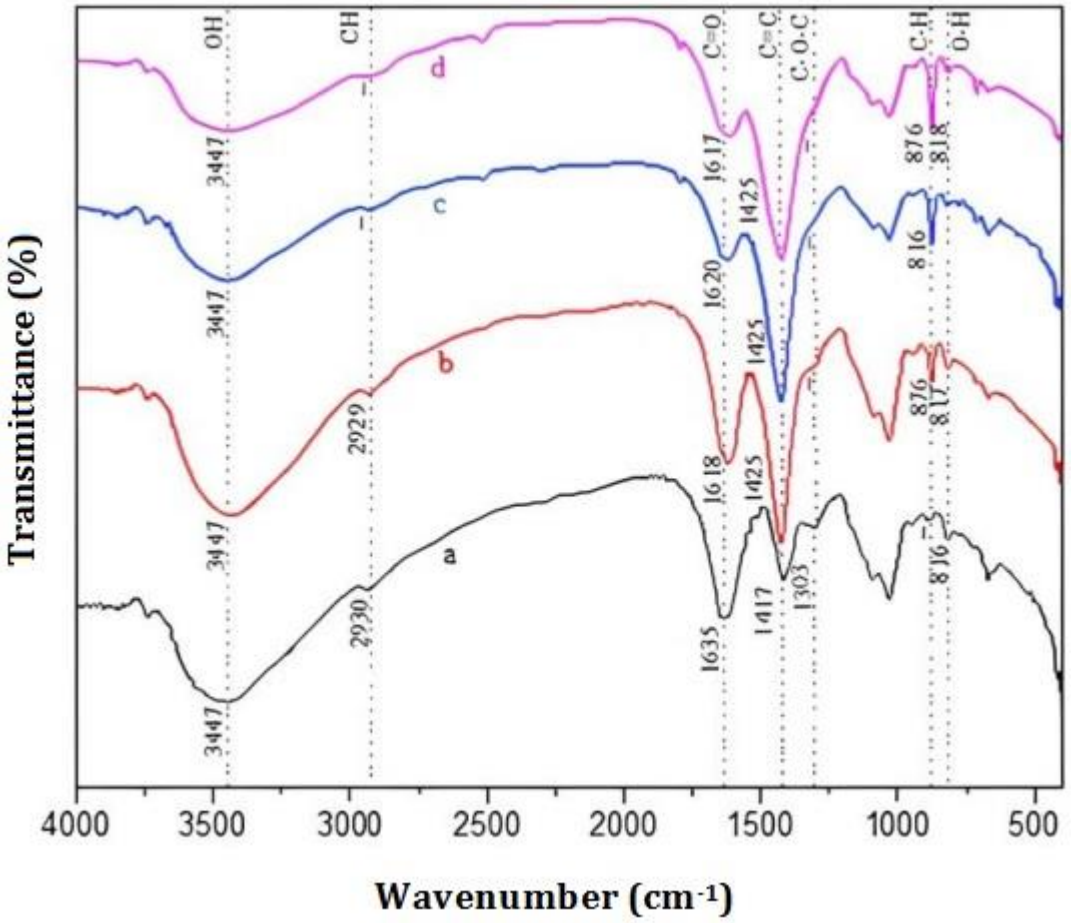

Figure 4: FTIR spectra of ACX beads (a) WP, (b) P-0.5, (c) P-1, and (d) P-1.5

Pore size was measured using image-J software, and the test results are summarized in Table 4. Table 4 presents ACX beads with higher porogen doses have larger pore diameters.

Based on the results of EDX, it is known that there are elements of Ca and Zn in the ACX beads with the addition of porogen. Ca elements indicate the presence of porogen $CaCO_3$ material in the ACX beads, and Zn elements indicate a crosslinking process between alginate and Zn^{2+}.

Optical microscope characterization

The shape of the ACX beads was observed using an optical microscope. The results of observations with an optical microscope are shown in Figure 8. ACX beads with porogen have a round shape, while ACX beads without porogen have an irregular shape. The more crosslinking processes that occur, the rounder the ACX beads will be. This is because alginates can form crosslinks with divalent cations such as Zn^{2+} and Ca^{2+}. The crosslinking process causes the formation of egg boxes in the alginate chain, as illustrated in Figure 9. The diameters of these ACX beads, crucial to understanding their structural properties and crosslinking effects, are detailed in Table 5. ACX beads diameter, where specific diameter measurements are given, providing insights into the size variations influenced by the presence or absence of porogen and the extent of crosslinking. Based on the data in Table 6, ACX beads without a porogen have a large diameter. ACX beads with a larger diameter have a greater swelling process.

Adsorption

The adsorption capacity is an important parameter to evaluate. Figure 10 shows that the maximum adsorption capacity is found in ACX beads with a contact time of 360 hours (142.47 mg g^{-1}).

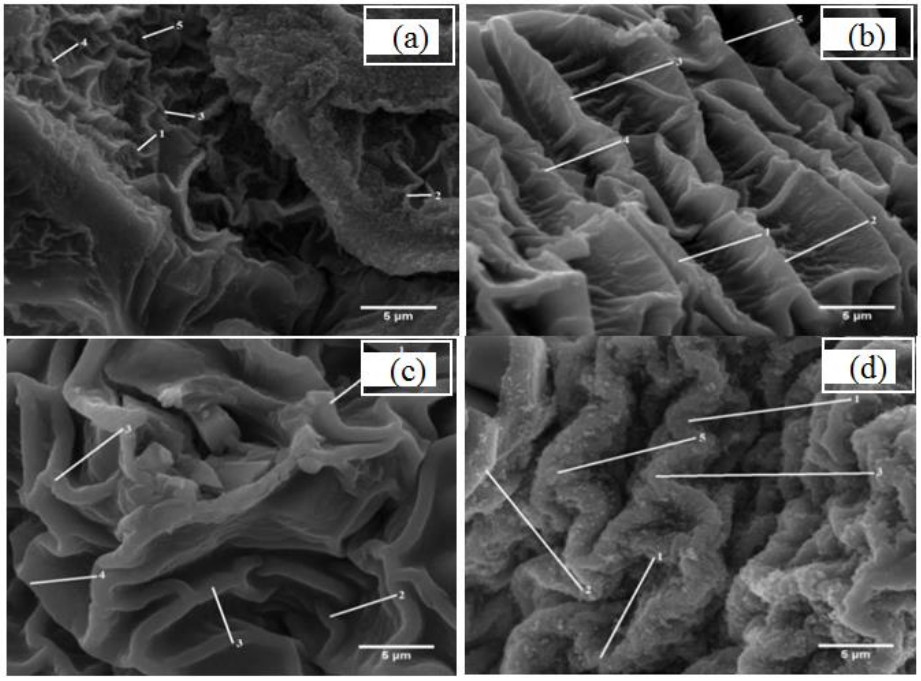

Figure 5: SEM image of ACX beads with magnification of 10,000x (a) WP, (b) P-0.5, (c) P-1, and (d) P-1.5

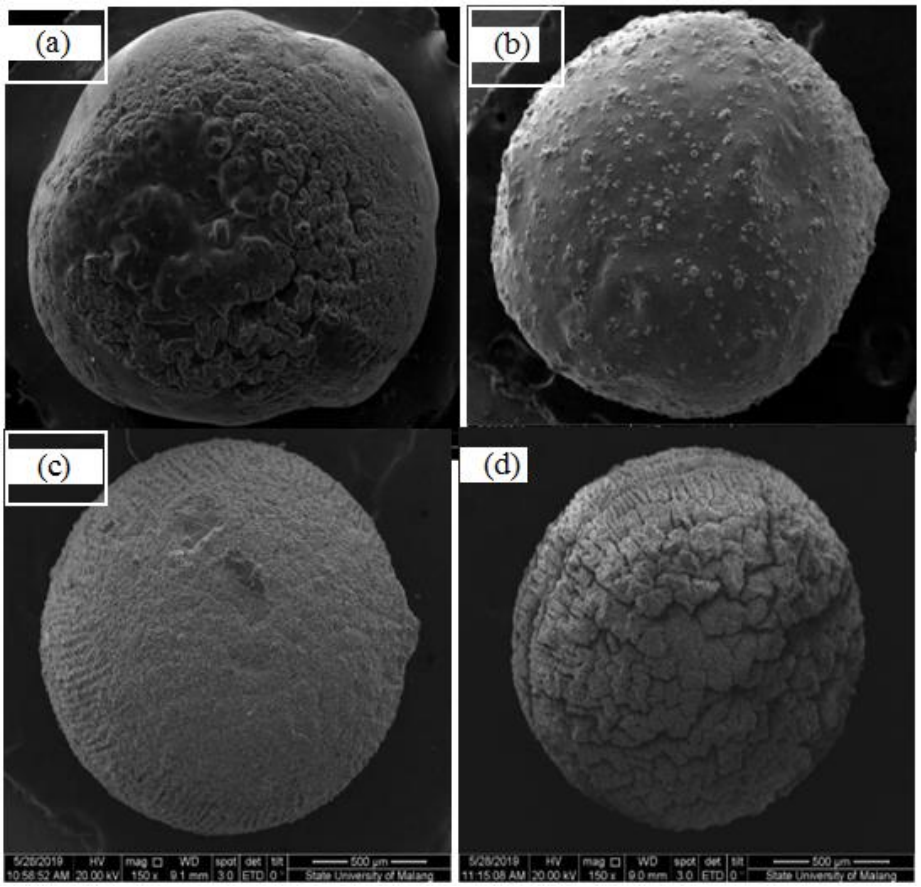

Figure 6: SEM image of ACX beads with the magnification of 150x (a) WP, (b) P-0.5, (c) P- 1, and (d) P-1.5

Table 3: Pore diameter range of ACX beads

WP (µm)	P-0.5 (µm)	P-1 (µm)	P-1.5 (µm)
2.535 – 3.425	2.922 – 5.086	4.120 – 5.628	7.171 – 10.291

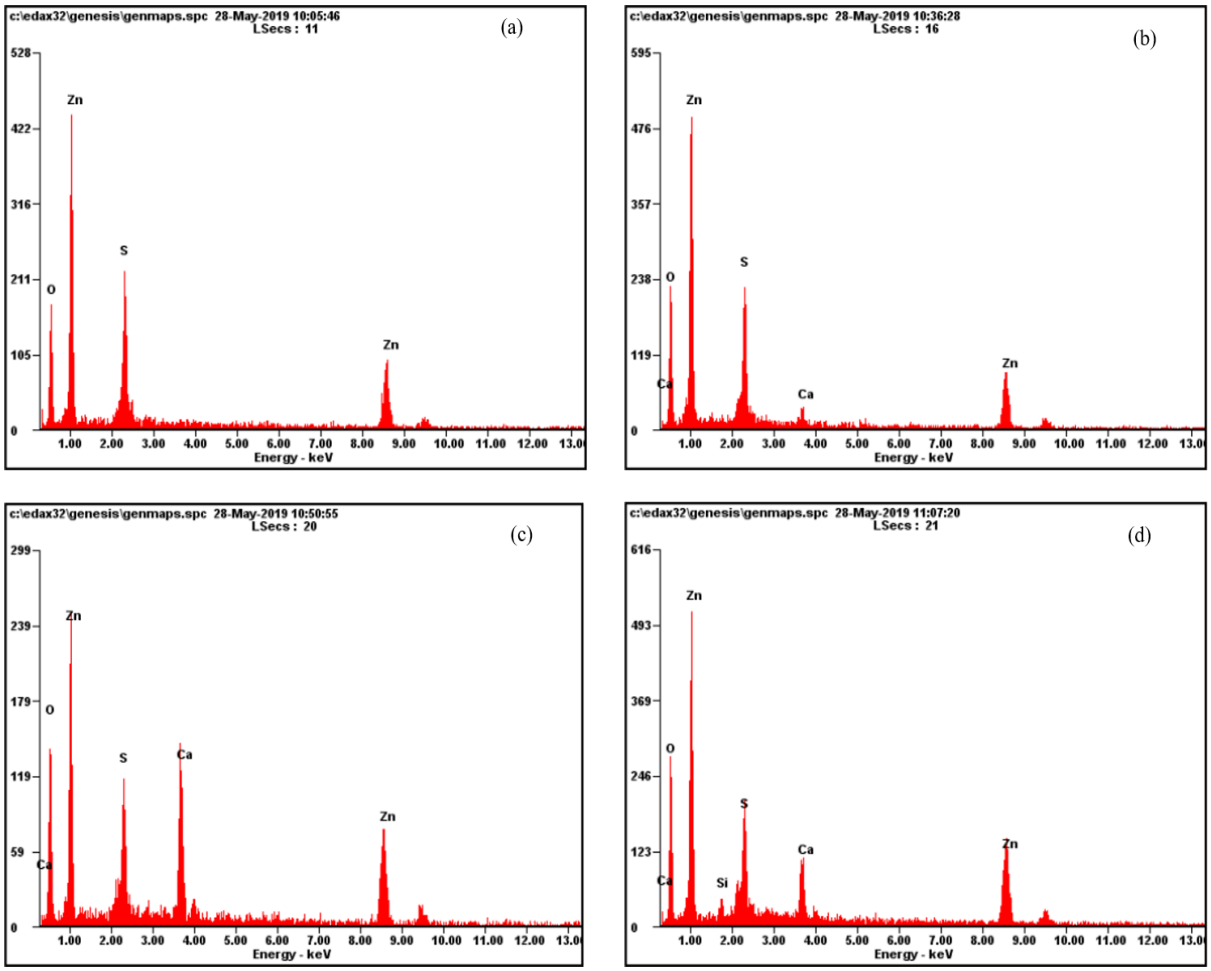

Figure 7: EDX spectra of ACX beads (a) without porogen, (b) porogen 0.5 g, (c) porogen 1 g, and (d) porogen 1.5 g

Table 4: Elemental content in ACX beads

ACX beads	%O	%S	%Ca	%Zn
WP	27.97	17.38	-	54.65
P-0.5	33.68	16.23	2.51	47.57
P-1	32.18	8.74	12.73	46.35
P-1.5	31.54	9.36	6.73	50.75

The adsorption capability decreases with an increasing porogen dosage. The increase in porogen dosage causes more crosslinks between divalent cations and alginate or cellulose so that the swelling is smaller, and this inhibits the bond between the ACX beads and methylene blue. In addition, the addition of the porogen $CaCO_3$ causes the pores to become larger [55, 56]. The pore size that is too large does not match the size of the methylene blue molecule, resulting in a decrease in adsorption capacity.

Adsorption kinetics

The adsorption kinetics provide important information about the controlling mechanisms of adsorption processes, such as mass transfer and chemical reaction. The adsorption kinetics of methylene blue on the surface of ACX beads were investigated using two kinetic models such as the pseudo-first order and pseudo-second order.

Pseudo-first order [57]:

$$\ln (qe - qt) = \ln qe - k_1 t \quad (1)$$

Pseudo-second order:

$$\frac{t}{qt} = \frac{1}{k_2 q_e^2} + \frac{t}{qe} \quad (2)$$

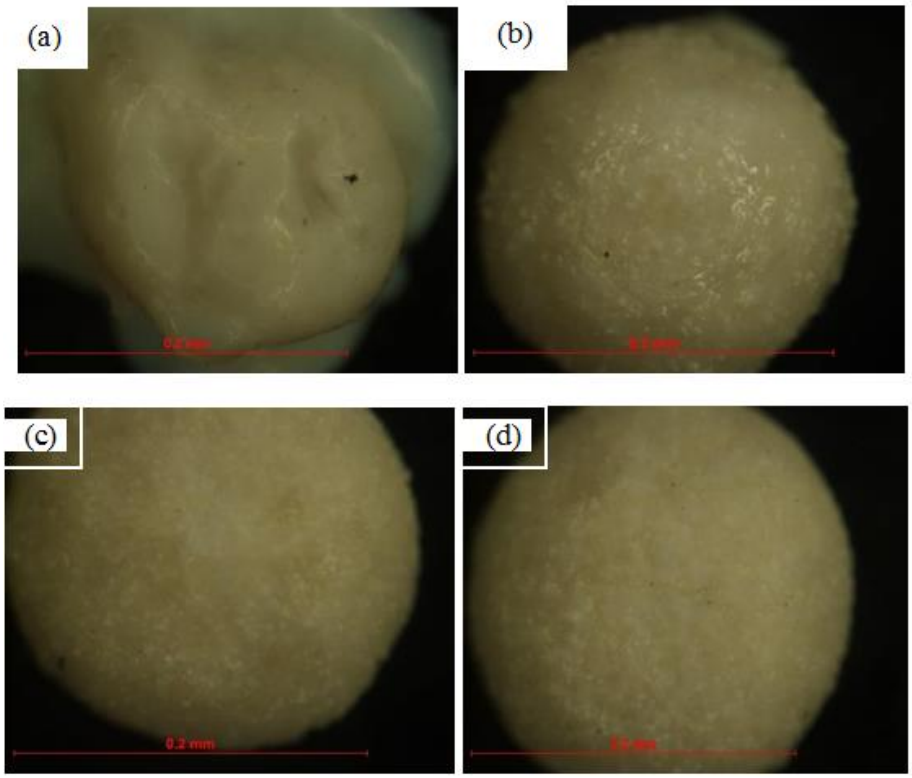

Figure 8: The optical microscope of ACX beads (a) WP, (b) P-0.5, (c) P-1, and (d) P-1.5

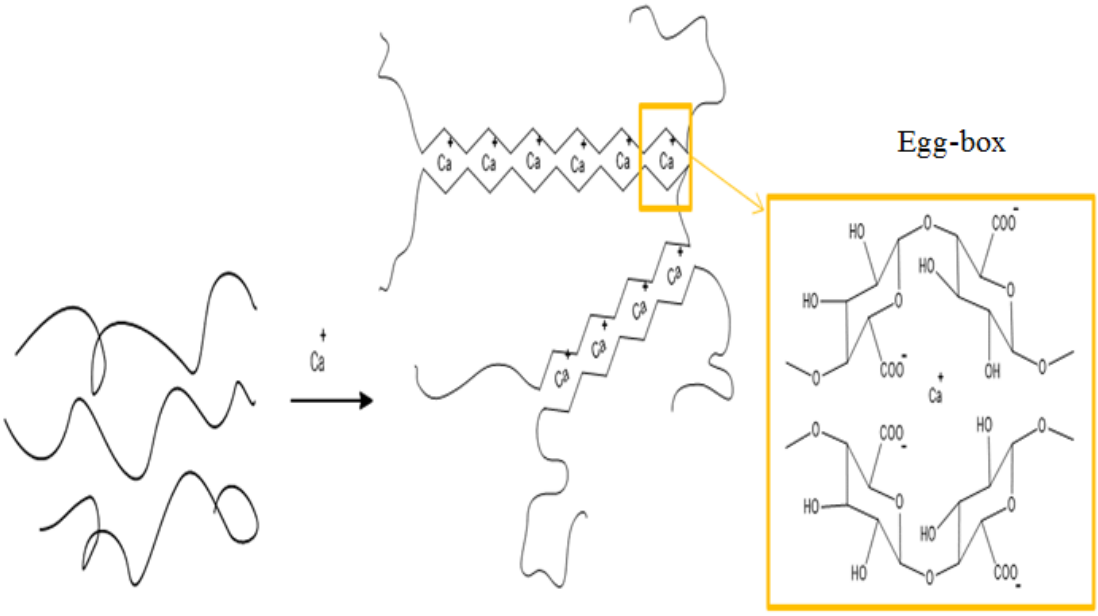

Figure 9: Interaction between cellulose xanthate beads and alginate reacting with calcium ions.

Table 5: ACX beads diameter

ACX beads	Dry ACX beads diameter* (mm)	Wet ACX beads diameter* (mm)
WP	1.873	5.657
P-0.5	1.838	5.571
P-1	1.204	4.814
P-1.5	1.658	4.186

** indicates the adsorbent amount (n = 10)*

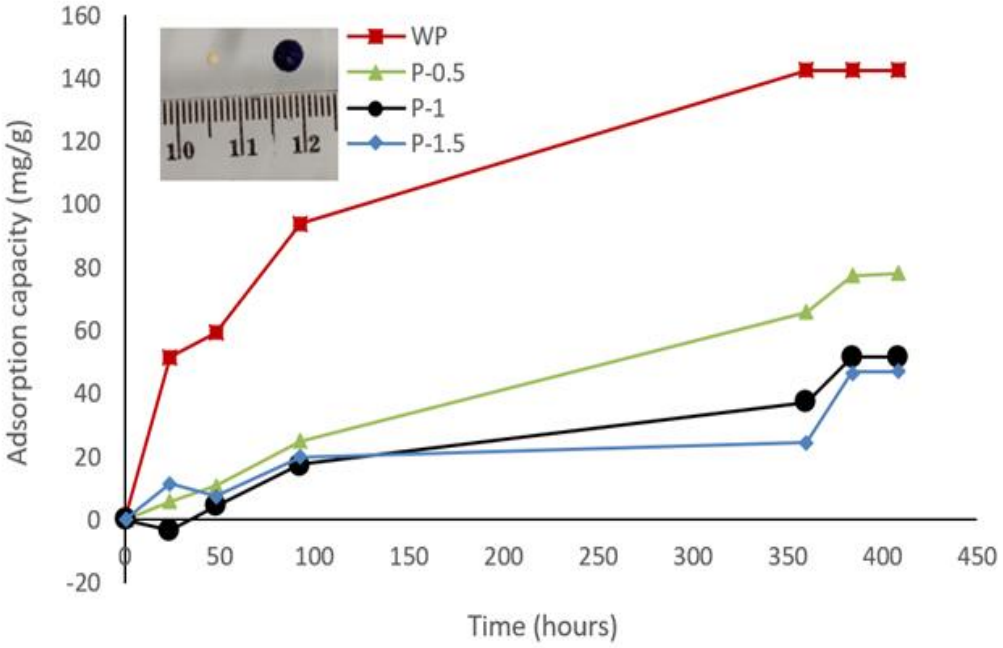

Figure 10: The adsorption capacity of ACX beads with variations in porogen dosage

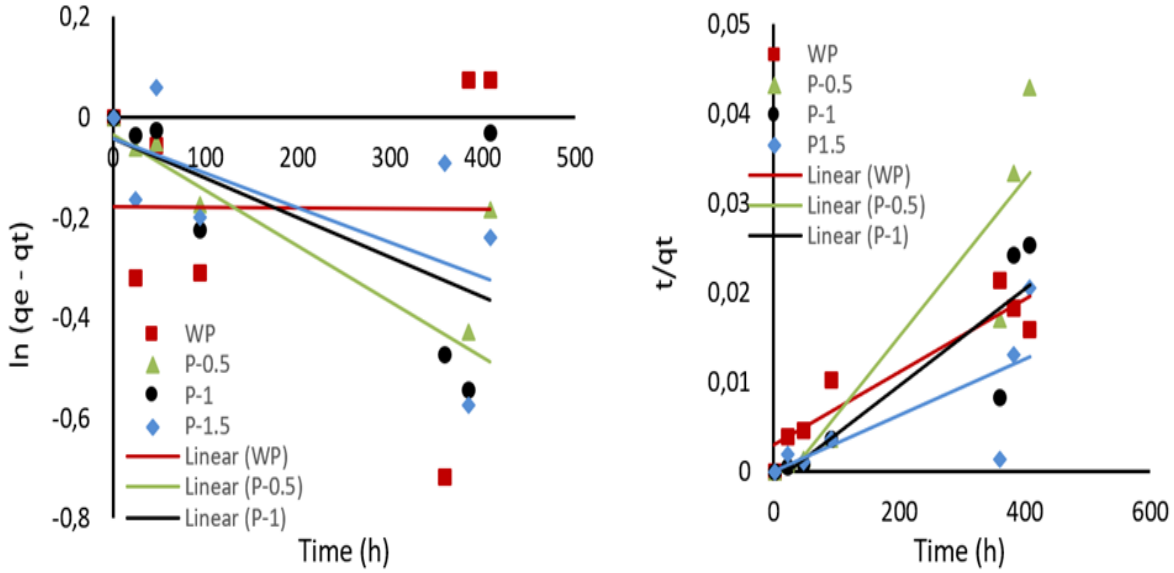

Figure 11: Kinetic curves of the (a) pseudo-first order and (b) pseudo-second order

Where, qe and qt are the absorption quantity of methylene blue per unit adsorbent ($mg \cdot g^{-1}$) at equilibrium and time t, respectively, k_1 (h^{-1}) and k_2 ($h \cdot g \cdot mg^{-1}$) are the rate constant for the pseudo-first-order and pseudo-second-order adsorption, respectively. The parameters of qe, k_1, and k_2 can be obtained experimentally from the slope and intercept of the plot of ln (qe - qt) or t/qt versus t.

The kinetic curves illustrating these models are depicted in Figure 11. Kinetic curves of the pseudo-first order (a) and pseudo-second order (b) visually represent the experimental data and the fitting of these two models, providing a clear understanding of the adsorption process dynamics on the ACX beads. The kinetic parameters are summarized in Table 6. It is noticed that the R^2 of the pseudo-second-order model is greater than those of the pseudo-first-order one. Accordingly, the pseudo second order model well describes the methylene blue adsorption on ACX beads where the rate limiting step is chemical adsorption.

Table 6: Adsorption kinetic parameters for methylene blue removal by ACX beads

Kinetics	ACX beads			
	WP	P-0.5	P-1	P-1.5
Pseudo-first-order				
qe	0.837	0.964	0.958	0.958
k_1	0.00001	0.0011	0.0008	0.001
R^2	0.00008	0.5167	0.4073	0.386
Pseudo-second-order				
qe	25000	11111	20000	33333
k_1	$0,6 \times 10^{-6}$	$-3,2 \times 10^{-6}$	$-1,9 \times 10^{-6}$	30×10^{-6}
R^2	0.8749	0.8631	0.8104	0.5584

Conclusion

This investigation aimed to synthesize ACX beads from corn stalks to remove methylene blue from an aqueous solution. ACX beads with various porogen dosages were printed using the ionic gelation method and then characterized using FTIR, an optical microscope, and SEM-EDX. The results of the FTIR analysis reported that in the cellulose xanthate spectrum, there was a change in the C-S, C=S, and S-C-S vibrations, which indicated that xanthate had formed. The optical microscope analysis showed that porogen made ACX beads round, while ACX beads without porogen's had irregular shapes. SEM-EDX analysis showed that the higher the porogen dosage, the rougher the surface morphology of the ACX beads and the larger the pore diameter. The presence of Ca in ACX beads with porogen indicates the presence of $CaCO_3$. Meanwhile, the presence of Zn indicates that the crosslinking process between alginate and Zn^{2+} has been formed. The maximum adsorption capacity was obtained on ACX beads without porogen with a contact time of 360 h. The study reveals that the kinetic adsorption followed a pseudo-second-order kinetic model proposed chemical adsorption. The adsorption capability decreases with an increasing porogen dosage. The increase in porogen dosage causes more crosslinks between divalent cations and alginate or cellulose, which inhibits the bond between the ACX beads and methylene blue. In addition, if the pore size is too large, it does not match the size of the methylene blue molecule.

Disclosure Statement

No potential conflict of interest was reported by the authors.

Funding

This research did not receive any specific grant from funding agencies in the public, commercial, or not-for-profit sectors.

Authors' Contributions

All authors contributed to data analysis, drafting, and revising of the paper and agreed to be responsible for all the aspects of this work.

ORCID

Eny Yulianti
https://orcid.org/0000-0002-4182-7720
Nanang Qazim
https://orcid.org/0009-0009-4081-0220
Anton Prasetyo
https://orcid.org/0000-0003-1575-8634
Siska Ela Kartika
https://orcid.org/0009-0003-9427-0393
Muhajidin Ahmad
https://orcid.org/0009-0007-2160-5753
Rahadian Zainul
https://orcid.org/0000-0002-3740-3597
Azril
https://orcid.org/0000-0001-8685-5517
Herland Satriawan
https://orcid.org/0009-0007-2398-4793
Ahmad Zikri
https://orcid.org/0000-0002-6933-7379
Mohammad Abdullah
https://orcid.org/0000-0003-1775-7926

References

[1]. Ryser L., Halseth G., Markey S., Moving from government to governance: Addressing housing pressures during rapid industrial development in Kitimat, BC, Canada, *Housing Studies*, 2021, **36**:1618 [Crossref], [Google Scholar], [Publisher]

[2]. Fan P., Yue W., Zhang J., Huang H., Messina J., Verburg P.H., Qi J., Moore N., Ge J., The spatial restructuring and determinants of industrial landscape in a mega city under rapid urbanization, *Habitat International*, 2020, **95**:102099 [Crossref], [Google Scholar], [Publisher]

[3]. Gičević A., Hindija L., Karačić A., *CMBEBIH 2019: Proceedings of the International Conference on Medical and Biological Engineering, 16–18 May 2019, Banja Luka, Bosnia and Herzegovina*, Springer, 2019 [Publisher]

[4]. Chung K.T., Azo dyes and human health: A review, *Journal of Environmental Science and Health, Part C*, 2016, **34**:233 [Crossref], [Google Scholar], [Publisher]

[5]. Khan I., Saeed K., Zekker I., Zhang B., Hendi A.H., Ahmad A., Ahmad S., Zada N., Ahmad H., Shah L.A., Review on methylene blue: Its properties, uses, toxicity and photodegradation, *Water*, 2022, **14**:242 [Crossref], [Google Scholar], [Publisher]

[6]. Ananda S., Lubis A.P., Zainul R., Identification of Acid Red 73 (CI 27290) in Cosmetic Hair Dye Preparations by High-Performance Liquid Chromatography–Photo Diode Array, in *IOP Conference Series: Earth and Environmental Science.* 012016 (IOP Publishing) [Google Scholar], [Publisher]

[7]. Begum R., Najeeb J., Sattar A., Naseem K., Irfan A., Al-Sehemi A.G., Farooqi Z.H., Chemical reduction of methylene blue in the presence of nanocatalysts: a critical review, *Reviews in Chemical Engineering*, 2020, **36**:749 [Crossref], [Google Scholar], [Publisher]

[8]. Rasooly S.S., Anwer M., Tsnim G., A Review on Treatment Methods for Pesticide Contaminated Water, *Journal of Environmental Science e, Toxicology and Food Technology*, 2022, **16**:24 [Google Scholar], [Publisher]

[9]. MadJin H.M., Hashim N., Isa I.M., Hussein M.Z., Bakar S.A., Mamat M., Ahmad R., Zainul R., Synthesis and characterisation of zinc hydroxides nitrates–sodium dodecyl sulphate fluazinam nano hosts for release properties, *Journal of Porous Materials*, 2020, **27**:1467 [Crossref], [Google Scholar], [Publisher]

[10]. Hamid A., Rahmawati Z., Abdullah M., Purbaningtyas T.E., Rohmah F., Febriana I.D., The Influence of NaOH Activator Concentration on the Synthesis of Activated Carbon from Banana Peel for Pb (II) Adsorption, *EKSAKTA: Berkala Ilmiah Bidang MIPA*, 2022, **23**:158 [Crossref], [Google Scholar], [Publisher]

[11]. Cao Y., Cheng C.M., Chen C.W., Liu M., Wang C., Pan W.P., Abatement of mercury emissions in the coal combustion process equipped with a Fabric Filter Baghouse, *Fuel*, 2008, **87**:3322 [Crossref], [Google Scholar], [Publisher]

[12]. Crini G., Lichtfouse E., Advantages and disadvantages of techniques used for wastewater treatment, *Environmental Chemistry Letters*, 2019, **17**:145 [Crossref], [Google Scholar], [Publisher]

[13]. Abd Azis N., Isa I.M., Hashim N., Ahmad M.S., Yazid S.N.A.M., Saidin M.I., Si S.M., Zainul R., Ulianas A., Mukdasai S., Voltammetric determination of bisphenol a in the presence of uric acid using a zn/al-ldh-qm modified MWCNT paste electrode, *International Journal of Electrochemical Science*, 2019, **14**:10607 [Crossref], [Google Scholar], [Publisher]

[14]. Muammar A., Manullang M., Arjuna M., Retnaningrum E., Isolation of cellulolytic microbes from bio-slurry, *EKSAKTA: Berkala Ilmiah Bidang MIPA*, 2021, **22**:27 [Crossref], [Google Scholar], [Publisher]

[15]. Sharif S.N.M., Hashim N., Isa I.M., Bakar S.A., Saidin M.I., Ahmad M.S., Mamat M., Hussein M.Z., Zainul R., Polymeric nanocomposite-based herbicide of carboxymethyl cellulose coated-zinc/aluminium layered double hydroxide-quinclorac: a controlled release purpose for agrochemicals, *Journal of Polymers and the Environment*, 2021, **29**:1817 [Crossref], [Google Scholar], [Publisher]

[16]. Yi T., Zhao H., Mo Q., Pan D., Liu Y., Huang L., Xu H., Hu B., Song H., From cellulose to cellulose nanofibrils—A comprehensive review of the preparation and modification of cellulose

nanofibrils, *Materials*, 2020, **13**:5062 [Crossref], [Google Scholar], [Publisher]
[17]. Aini N.S., Murtadlo A.A.A., Tamam M.B., Turista D.D.R., Naw S.W., Ullah M.E., Triple Inhibitor Mechanism of Antiretroviral from Sambucus nigra Phytochemical through Screening Docking, *SAINSTEK International Journal on Applied Science, Advanced Technology and Informatics*, 2023, **2**:18 [Crossref], [Google Scholar], [Publisher]
[18]. Farhat W., Venditti R.A., Hubbe M., Taha M., Becquart F., Ayoub A., A review of water-resistant hemicellulose-based materials: processing and applications, *ChemSusChem*, 2017, **10**:305 [Crossref], [Google Scholar], [Publisher]
[19]. Amelia F., Yusmaita E., Fernanda Y., Yulianis F., Rahmayani S., Islam A., Assessing the Potentiality of Aerobic Rolling Composter to Hasten Vegetable and Fruit Waste, *EKSAKTA: Berkala Ilmiah Bidang MIPA*, 2023, **24**:92 [Crossref], [Google Scholar], [Publisher]
[20]. Khanjanzadeh H., Behrooz R., Bahramifar N., Gindl-Altmutter W., Bacher M., Edler M., Griesser T., Surface chemical functionalization of cellulose nanocrystals by 3-aminopropyltriethoxysilane, *International journal of biological macromolecules*, 2018, **106**:1288 [Crossref], [Google Scholar], [Publisher]
[21]. Iryani D.A., Risthy N.M., Resagian D.A., Yuwono S.D., Hasanudin U., Preparation and evaluation adsorption capacity of cellulose xanthate of sugarcane bagasse for removal heavy metal ion from aqueous solutions, in *IOP Conference Series: Earth and Environmental Science*, 2017, 012039 (IOP Publishing) [Google Scholar], [Publisher]
[22]. Sayyed A.J., Pinjari D.V., Sonawane S.H., Bhanvase B.A., Sheikh J., Sillanpää M., Cellulose-based nanomaterials for water and wastewater treatments: A review, *Journal of Environmental Chemical Engineering*, 2021, **9**:106626 [Crossref], [Google Scholar], [Publisher]
[23]. Abdelhamid H.N., Mathew A.P., Cellulose-based materials for water remediation: adsorption, catalysis, and antifouling, *Frontiers in Chemical Engineering*, 2021, **3**:790314 [Crossref], [Google Scholar], [Publisher]
[24]. Azizah N.W., Hidayah C.N., Latifah A.F., Yulianti E., Khoiroh L.M., Synthesis and Characterization of Alginate-Cellulose Xanthate Beads from Corn Stalk with Porogen Variation, in *Proceedings of the International Conference on Green Technology*, 2019, 54 Publisher]
[25]. Rahmadiawan D., Abral H., Ilham M.K., Puspitasari P., Nabawi R.A., Shi S.C., Sugiarti E., Muslimin A.N., Chandra D., Ilyas R., Enhanced UV blocking, tensile and thermal properties of bendable TEMPO-oxidized bacterial cellulose powder-based films immersed in PVA/Uncaria gambir/ZnO solution, *Journal of materials research and technology*, 2023, **26**:5566 [Crossref], [Google Scholar], [Publisher]
[26]. Rahmadiawan D., Abral H., Shi S.C., Ilham M.K., Sugiarti E., Muslimin A.N., Ilyas R., Zainul R., Effect of Different Types of Preparation Methods on the Properties of Tempo-Oxidized Bacterial Cellulose Powder Film, *Available at SSRN 4470819* [Crossref], [Google Scholar], [Publisher]
[27]. Wang J., Yang Z., Xu J., Ahmad M., Zhang H., Zhang A., Zhang Q., Kou X., Zhang B., Surface microstructure regulation of porous polymer microspheres by volume contraction of phase separation process in traditional suspension polymerization system, *Macromolecular Rapid Communications*, 2019, **40**:1800768 [Crossref], [Google Scholar], [Publisher]
[28]. Foroughirad S., Haddadi-Asl V., Khosravi A., Salami-Kalajahi M., Effect of porogenic solvent in synthesis of mesoporous and microporous molecularly imprinted polymer based on magnetic halloysite nanotubes, *Materials Today Communications*, 2021, **26**:101780 [Crossref], [Google Scholar], [Publisher]
[29]. Rohmatullah W.A.P., Yulianti E., Khoiroh L.M., Mahmudah R.a., Synthesis and characterization of alginate-cellulose xanthate beads from corn stalk with NACL as porogen, in *Annales Bogorienses.* (LIPI), 2020 [Google Scholar], [Publisher]
[30]. Wei J., Zhang S., Yuan J., Wang Z., Zong S., Cui Y., Nanoscale imaging of tumor cell exosomes by expansion single molecule localization microscopy (ExSMLM), *Talanta*, 2023, **261**:124641 [Crossref], [Google Scholar], [Publisher]
[31]. Pandey L.M., Enhanced adsorption capacity of designed bentonite and alginate beads for the effective removal of methylene blue, *Applied Clay*

Science, 2019, **169**:102 [Crossref], [Google Scholar], [Publisher]
[32]. Putri G.E., Gusti F.R., Sary A.N., Zainul R., Synthesis of silver nanoparticles used chemical reduction method by glucose as reducing agent, in *Journal of Physics: Conference Series*, 2019 012027 (IOP Publishing) [Google Scholar], [Publisher]
[33]. El Hajj J., Nguyen E., Liu Q., Bouyer C., Adriaenssens E., Hilal G., Ségal-Bendirdjian E., Telomerase regulation by the long non-coding RNA H19 in human acute promyelocytic leukemia cells, *Molecular cancer*, 2018, **17**:1 [Crossref], [Google Scholar], [Publisher]
[34]. Iskandar I., Horiza H., Bacterial Isolation Which is Potential as Cellulosa Pedegradation in Coastal Performance In Tanjungpinang City, *EKSAKTA: Berkala Ilmiah Bidang MIPA*, 2019, **20**:70 [Crossref], [Google Scholar], [Publisher]
[35]. Miao Y., Zhi Y., Zhang H., Chen Y., Shan S., Jia Q., Ni Y., Recycled fiber treated with NaOH/urea aqueous solution: effects on physical properties of paper sheets and on hornification, *Nordic Pulp & Paper Research Journal*, 2018, **33**:651 [Crossref], [Google Scholar], [Publisher]
[36]. Wang H., Chen C., Fang L., Li S., Chen N., Pang J., Li D., Effect of delignification technique on the ease of fibrillation of cellulose II nanofibers from wood, *Cellulose*, 2018, **25**:7003 [Crossref], [Google Scholar], [Publisher]
[37]. Rohmatullah W.A.P., Yulianti E., Khoiroh L.M., Mahmudah R.a., Synthesis And Characterization Of Alginate-Cellulose Xanthate Beads From Corn Stalk With NaCL As Porogen, in *Annales Bogorienses.* (LIPI), 2021, **24**:59 [Google Scholar], [Publisher]
[38]. Khusna L.N., Yulianti E., Khoiroh L.M., Istighfarini V.N., Synthesis and Characterization of Beads Alginate Carboxymethyl Cellulose from Corn Stalk (Zea Mays) Using $BaCl_2$ as Crosslink with Variation Concentration, in *International Conference on Engineering, Technology and Social Science (ICONETOS 2020)*, 2021, 383 (Atlantis Press). [Crossref], [Google Scholar], [Publisher]
[39]. Lisuzzo L., Cavallaro G., Parisi F., Milioto S., Fakhrullin R., Lazzara G., Core/shell gel beads with embedded halloysite nanotubes for controlled drug release, *Coatings*, 2019, **9**:70 [Crossref], [Google Scholar], [Publisher]
[40]. Qin C., Zhou J., Zhang Z., Chen W., Hu Q., Wang Y., Convenient one-step approach based on stimuli-responsive sol-gel transition properties to directly build chitosan-alginate core-shell beads, *Food hydrocolloids*, 2019, **87**:253 [Crossref], [Google Scholar], [Publisher]
[41]. L. Dantas M.J., F. dos Santos B.F., A. Tavares A., Maciel M.A., Lucena B.d.M., L. Fook M.V., de L. Silva S.M., The impact of the ionic cross-linking mode on the physical and in vitro dexamethasone release properties of chitosan/hydroxyapatite beads, *Molecules*, 2019, **24**:4510 [Crossref], [Google Scholar], [Publisher]
[42]. Mushtaq F., Raza Z.A., Batool S.R., Zahid M., Onder O.C., Rafique A., Nazeer M.A., Preparation, properties, and applications of gelatin-based hydrogels (GHs) in the environmental, technological, and biomedical sectors, *International journal of biological macromolecules*, 2022 [Crossref], [Google Scholar], [Publisher]
[43]. Alamin N.U., Khan A.S., Nasrullah A., Iqbal J., Ullah Z., Din I.U., Muhammad N., Khan S.Z., Activated carbon-alginate beads impregnated with surfactant as sustainable adsorbent for efficient removal of methylene blue, *International journal of biological macromolecules*, 2021, **176**:233 [Crossref], [Google Scholar], [Publisher]
[44]. Njaramba L.K., Kim S., Kim Y., Cha B., Kim N., Yoon Y., Park C.M., Remarkable adsorption for hazardous organic and inorganic contaminants by multifunctional amorphous core–shell structures of metal–organic framework-alginate composites, *Chemical Engineering Journal*, 2022, **431**:133415 [Crossref], [Google Scholar], [Publisher]
[45]. Esparza-Flores E.E., Siquiera L.B., Cardoso F.D., Costa T.H., Benvenutti E.V., Medina-Ramírez I.E., Perullini M., Santagapita P.R., Rodrigues R.C., Hertz P.F., Chitosan with modified porosity and crosslinked with genipin: A dynamic system structurally characterized, *Food hydrocolloids*, 2023, **144**:109034 [Crossref], [Google Scholar], [Publisher]
[46]. Cipitria A., Boettcher K., Schoenhals S., Garske D.S., Schmidt-Bleek K., Ellinghaus A., Dienelt A., Peters A., Mehta M., Madl C.M., In-situ tissue regeneration through SDF-1α driven cell recruitment and stiffness-mediated bone

regeneration in a critical-sized segmental femoral defect, *Acta biomaterialia*, 2017, **60**:50 [Crossref], [Google Scholar], [Publisher]
[47]. Nasrullah A., Bhat A., Naeem A., Isa M.H., Danish M., High surface area mesoporous activated carbon-alginate beads for efficient removal of methylene blue, *International journal of biological macromolecules*, 2018, **107**:1792 [Crossref], [Google Scholar], [Publisher]
[48]. Fitri E., Effendi E., Azra A., Utilization of Dry Cocoa Pod Husks as an Antioxidant-Rich Herbal Drink, *EKSAKTA: Berkala Ilmiah Bidang MIPA*, 2021, **22**:102 [Crossref], [Google Scholar], [Publisher]
[49]. Hasanudin H., Asri W.R., Zulaikha I.S., Ayu C., Rachmat A., Riyanti F., Hadiah F., Zainul R., Maryana R., Hydrocracking of crude palm oil to a biofuel using zirconium nitride and zirconium phosphide-modified bentonite, *RSC advances*, 2022, **12**:21916 [Crossref], [Google Scholar], [Publisher]
[50]. Sharif S.N., Hashim N., Isa I.M., Bakar S.A., Saidin M.I., Ahmad M.S., Mamat M., Hussein M.Z., Zainul R., Chitosan as a coating material in enhancing the controlled release behaviour of zinc hydroxide nitrate–sodium dodecylsulphate–bispyribac nanocomposite, *Chemical Papers*, 2021, **75**:611 [Crossref], [Google Scholar], [Publisher]
[51]. Iryani D.A., Risthy N.M., Resagian D.A., Yuwono S.D., Hasanudin U., Preparation and evaluation adsorption capacity of cellulose xanthate of sugarcane bagasse for removal heavy metal ion from aqueous solutions, in *IOP Conference Series: Earth and Environmental Science*, 2017, 012039 (IOP Publishing). [Google Scholar], [Publisher]
[52]. Iqbal J., Shah N.S., Sayed M., Imran M., Muhammad N., Howari F.M., Alkhoori S.A., Khan J.A., Khan Z.U.H., Bhatnagar A., Synergistic effects of activated carbon and nano-zerovalent copper on the performance of hydroxyapatite-alginate beads for the removal of As3+ from aqueous solution, *Journal of Cleaner Production*, 2019, **235**:875 [Crossref], [Google Scholar], [Publisher]
[53]. Ghorpade V.S., Yadav A.V., Dias R.J., Citric acid crosslinked cyclodextrin/hydroxypropylmethylcellulose hydrogel films for hydrophobic drug delivery, *International journal of biological macromolecules*, 2016, **93**:75 [Crossref], [Google Scholar], [Publisher]
[54]. Sun X.F., Zeng Q., Wang H., Hao Y., Preparation and swelling behavior of pH/temperature responsive semi-IPN hydrogel based on carboxymethyl xylan and poly (N-isopropyl acrylamide), *Cellulose*, 2019, **26**:1909 [Crossref], [Google Scholar], [Publisher]
[55]. Sinha V., Chakma S., Advances in the preparation of hydrogel for wastewater treatment: A concise review, *Journal of Environmental Chemical Engineering*, 2019, **7**:103295 [Crossref], [Google Scholar], [Publisher]
[56]. Mohd Sharif S.N., Hashim N., Md Isa I., Abu Bakar S., Idris Saidin M., Syahrizal Ahmad M., Mamat M., Zobir Hussein M., Zainul R., Carboxymethyl cellulose hydrogel based formulations of zinc hydroxide nitrate-sodium dodecylsulphate-bispyribac nanocomposite: Advancements in controlled release formulation of herbicide, *Journal of nanoscience and nanotechnology*, 2021, **21**:5867 [Crossref], [Google Scholar], [Publisher]
[57]. Zhao J., Yu L., Ma H., Zhou F., Yang K., Wu G., Corn stalk-based activated carbon synthesized by a novel activation method for high-performance adsorption of hexavalent chromium in aqueous solutions, *Journal of colloid and interface science*, 2020, **578**:650 [Crossref], [Google Scholar], [Publisher]

HOW TO CITE THIS ARTICLE
Eny Yulianti, Nanang Qazim, Anton Prasetyo, Siska Ela Kartika, Muhajidin Ahmad, Rahadian Zainul, Azril, Herland Satriawan, Ahmad Zikri, Mohammad Abdullah. Investigation of Calcium Carbonate Porogen on Methylene Blue Adsorption in Alginate Cellulose Xanthate Beads from Corn Stalks. *J. Med. Chem. Sci.*, 2024, 7(3) 538-554.
DOI: https://doi.org/10.26655/JMCHEMSCI.2024.3.9
URL: https://www.jmchemsci.com/article_185083.html